




Fission fragment mass and folding angle distributions in the reaction ${}^9\text{Be} + {}^{238}\text{U}$

D. Paul ^{1,2} A. Sen ^{1,2} T. K. Ghosh ^{1,2,*} Md. Moin Shaikh,^{1,†} K. Atreya,^{1,2} Rajkumar Santra,^{2,3} Samir Kundu,^{1,2} T. K. Rana,^{1,2} K. Banerjee,^{1,2} C. Bhattacharya,^{1,2} S. Bhattacharya,^{1,‡} J. K. Meena,¹ D. C. Biswas,^{2,4} B. N. Joshi,⁴ N. Kumar,^{2,4} G. K. Prajapati,^{2,4} Y. K. Gupta,^{2,4} K. Mahata,^{2,4} K. Ramachandran,⁴ and S. Pal⁵

¹Variable Energy Cyclotron Centre, 1/AF, Bidhan Nagar, Kolkata 700064, India

²Homi Bhabha National Institute, Training School Complex, Anushakti Nagar, Mumbai 400094, India

³Saha Institute of Nuclear Physics, 1/AF, Bidhan Nagar, Kolkata 700064, India

⁴Nuclear Physics Division, Bhabha Atomic Research Centre, Mumbai 400085, India

⁵Tata Institute of Fundamental Research, Navy Nagar, Colaba, Mumbai 400005, India



(Received 24 March 2021; accepted 21 July 2021; published 6 August 2021)

Background: The excitation energy dependence of the fission fragment mass and folding angle distributions for reactions with loosely bound projectiles are reported to be significantly different compared to the reactions with tightly bound nuclei. Extensive study to understand the reaction mechanism of weakly bound projectiles is required as it can simulate the mechanism of fission induced with radioactive ion beams.

Purpose: The effect of loosely bound nuclei on fission fragment folding angle and mass distributions in the ${}^9\text{Be} + {}^{238}\text{U}$ reaction near the Coulomb barrier energies is investigated and the contributions of incomplete fusion fission in the total fission cross section are studied.

Methods: Mass and folding angle distributions of the fission fragments have been measured near the Coulomb barrier energies using two large area multiwire proportional counters. Fragment masses were determined from the time-of-flight difference method. To understand the effect of breakup of loosely bound nuclei, the results are compared with tightly bound proton-, α -particle-, and carbon-induced reactions, as well as with the predictions from semiempirical calculations.

Results: The width of folding angle distributions is found to increase with lowering excitation energy in the ${}^9\text{Be} + {}^{238}\text{U}$ reaction. This is in contrast to the reaction ${}^{12}\text{C} + {}^{232}\text{Th}$ involving tightly bound projectiles, populating similar compound nuclei. The peak-to-valley ratios of the fission fragment mass distributions for all events are found to sharply increase with lowering excitation energy in the ${}^9\text{Be} + {}^{238}\text{U}$ reaction. The possible contribution of incomplete fusion into the total fission cross section could be extracted. The measured mass distributions were found to be consistent with the semiempirical calculation GEF and macro-microscopic two-center shell model calculations considering the admixture of incomplete fusion fission.

Conclusion: For actinide targets, mass distributions of inclusive fission are influenced by the breakup/transfer channels of the weakly bound projectiles. At the above-barrier energies, the contribution of incomplete fusion is found to be $\approx 25 \pm 4\%$ which is similar to the reported value of the complete fusion suppression factor in reactions involving nuclei with low binding energies. The increase in the peak-to-valley ratio with lowering excitation energy in the fission fragment mass distribution could be explained by the combined analysis of folding angle and mass distributions.

DOI: [10.1103/PhysRevC.104.024604](https://doi.org/10.1103/PhysRevC.104.024604)

I. INTRODUCTION

Recent experiments carried out worldwide with loosely bound projectiles mostly concentrate on the effect of their unique structural features such as weak binding, extended spatial distribution, clustering, etc., on the fusion process [1–5]. Intuitively, the extended spatial distribution of the neutrons of weakly bound neutron-rich nuclei should cause nuclear overlap at a relatively larger distance, and thereby lower the

Coulomb barrier during the fusion process. Therefore, the subbarrier fusion cross section is expected to be enhanced [6]. On the contrary, the breakup of loosely bound nuclei in the Coulomb field of the target nucleus could prevent the capture of the whole projectile, thereby inhibiting the complete fusion process [7]. No enhancement of cross section has also been reported at energies below the Coulomb barrier in fusion with light unstable nuclei, making the picture more contradictory [8,9].

However, several studies near and above the barrier with stable loosely bound nuclei [10–13] conclusively indicated that the incomplete fusion-fission (ICF) mechanism strongly modifies the complete fusion-fission (CF) yield, causing a reduction of $\approx 30\%$ of the calculated CF cross section. For loosely bound light projectiles with prominent cluster

*tilak@vecc.gov.in

†Present address: Department of Physics, Chanchal College, Chanchal, Malda, West Bengal 732123, India.

‡Retired.

structures, breakup capture, direct breakup, and direct transfer (cluster and nucleon) are considered to be the most significant processes contributing to incomplete fusion yield [14,15]. Several experiments have been performed in recent years using various probes [e.g., fission fragment (FF) mass and folding angle distributions [10,11], correlation of light projectile-like particles emitted in coincidence with a light particle/fission fragment [12], etc.) to investigate the relative contribution of each of the processes mentioned above in the ICF yield.

The presence of incomplete fusion can be studied from the fission fragment folding angle and mass distributions [16,17]. Here, the shift in folding angle distribution and the change in peak-to-valley ratio of the fission fragment mass distribution with respect to those predicted for CF are usually used to extract the ICF yield. From the measurement of fission fragment folding angle distributions in the reaction ${}^6\text{Li} + {}^{232}\text{Th}$, Itkis *et al.* [10] showed that the ICF originates from transfer and breakup reactions, and the contribution of complete fusion into the total fusion fission cross section is about 27% at 2 MeV below the Coulomb barrier. The study of fission fragment folding angle distributions and peak-to-valley ratio of the fission fragment mass distributions for ${}^{6,7}\text{Li} + {}^{238}\text{U}$ reactions [18] indicated a different behavior compared to those for the reactions with tightly bound projectiles. This was understood by assuming additional contributions of breakup/transfer-induced fission in reactions with loosely bound projectiles at near-barrier energies. Coincident measurements of light charged particle fission fragments for several systems involving loosely bound projectiles (${}^{6,7}\text{Li}$, ${}^{7,9}\text{Be}$) and heavy targets (${}^{209}\text{Bi}$, ${}^{232}\text{Th}$, ${}^{238}\text{U}$) have also indicated large ($\approx 20\text{--}30\%$) suppression of complete fusion yield at above-barrier energies in all cases, and attributed the suppression to an incomplete fusion process resulting primarily from direct cluster transfer processes [1,2,11,12].

From the above studies, it is clear that the intricacies of the fusion process should be thoroughly understood through detailed systematic studies, as they may provide important hints that could be extremely helpful in the endeavor to reach the super heavy island using fusion reactions with loosely bound radioactive beams. Here, we report the fission fragment folding angle and mass distributions in a reaction with loosely bound nucleus ${}^9\text{Be}$ on the actinide target ${}^{238}\text{U}$ at energies near the Coulomb barrier. To understand the effect of breakup, we compare the present results in reactions with those obtained using tightly bound projectiles to populate a similar compound nucleus ${}^{244}\text{Cm}$. The data were also compared with proton- and α -particle-induced fission of ${}^{238}\text{U}$, where no contribution of ICF is expected. From the combined analysis of these distributions, the contribution of ICF in total fission cross sections of the ${}^9\text{Be} + {}^{238}\text{U}$ system was estimated. The measured mass distributions were compared to the predictions of the semiempirical calculation in GEF [19], as well as macro-microscopic two-center shell model calculations [20].

II. EXPERIMENTAL DETAILS

The experiment was performed using the ${}^9\text{Be}$ pulsed beam from the BARC-TIFR Pelletron facility in Mumbai, India.

A ${}^{238}\text{U}$ target of thickness $200\ \mu\text{g}/\text{cm}^2$ on ${}^{\text{nat}}\text{C}$ backing of thickness $20\ \mu\text{g}/\text{cm}^2$ was used. Two position-sensitive multiwire proportional counter (MWPC) detectors [21] were mounted 25.8 cm and 15.7 cm away from the target position. Each of the detectors had an active area of $17.5 \times 7\ \text{cm}^2$. Angular positions of the forward and backward detectors were 54° and 120° , respectively, with respect to the beam axis. These angles were selected from Viola systematics [22] corresponding to full momentum transfer of the projectile to the compound nucleus. The forward detector had an angular coverage of 44° and the backward detector had an angular coverage of 72° . The target plane was kept in the orientation of 45° with respect to the beam axis, to avoid the shadowing of the detectors.

The detectors were operated at 3 Torr pressure of isobutane gas so that elastic and quasielastic particles pass through the detectors. The position information (X, Y), energy loss in the detectors, and time of flight of the fission fragments with respect to the pulsed beam were recorded event by event by using a VME-based data acquisition system. The counts from the Faraday cup were used to normalize the data and monitor the beam flux. Using the time-of-flight (TOF) difference method, the masses of the complementary fragments were determined. The mass resolution of the experimental setup was $\approx 5\ \text{u}$. The method of calculation of the fission fragment masses is described in detail in Refs. [23,24].

III. RESULTS AND DISCUSSION

The fission fragment folding angle and mass distributions in the reaction ${}^9\text{Be} + {}^{238}\text{U}$ were measured at energies $E_{\text{lab}} = 37.5, 39, 42, \text{ and } 47\ \text{MeV}$ near the Coulomb barrier ($V_B = 44.7\ \text{MeV}$). Complete and incomplete fusion cross sections were separated from the combined analysis of the mass and folding angle distributions.

A. Folding angle distributions

In Figs. 1(a)–1(d), we show the typical fission fragment folding angle distributions in the reaction plane (θ) versus out of the plane (ϕ) at below-, near-, and above-barrier energies. The projections of the folding angles on the reaction plane are shown in Figs. 1(e)–1(h). The peaks of the folding angle distributions were found to be consistent with the calculated values (as shown by the red arrow in Fig. 1) for the full momentum transfer of the projectile. However, it can be observed that the shape of the fission fragment folding angle at the subbarrier energy is different compared to that at above-barrier energies. At $E_{\text{lab}} = 37.5\ \text{MeV}$, the prominent “shoulder” at the right side of the folding angle distribution (shown by the dashed blue arrow) is due to the relatively higher contribution of the incomplete fusion process, in which a part of the projectile, namely, a neutron, is captured by the target nucleus after breakup of ${}^9\text{Be}$ into two ${}^4\text{He}$ atoms and a neutron. In this case, the neutron-induced fission fragment folding angle is peaked around 180° and is larger than that from the CF fission process.

The folding angle distribution of the fission fragments is sensitive to the transfer of momentum from the projectile to

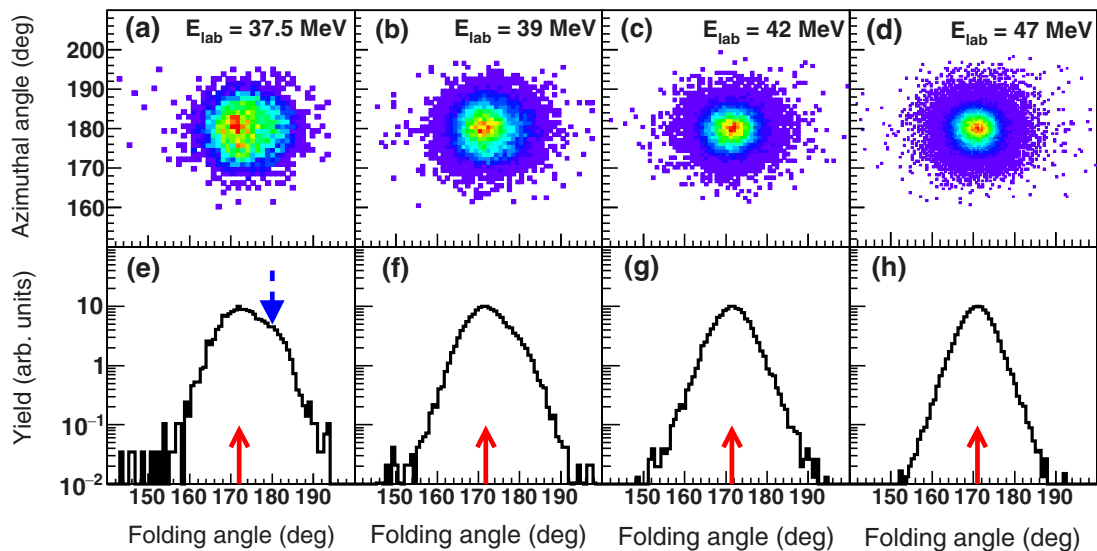


FIG. 1. Folding angle distributions for the reaction ${}^9\text{Be} + {}^{238}\text{U}$ at measured beam energies of $E_{\text{lab}} = 37.5, 39, 42,$ and 47 MeV.

the target. Hence, an analysis of the folding angle distribution of reactions induced by weakly bound projectiles of ${}^9\text{Be}$ is indicative of the presence of ICF in the reaction [10,25]. The measured width of the folding angle distribution in the case of complete fusion fission is influenced by the detector opening angle, the shape of the mass distribution of the fission fragments (e.g., whether symmetric or asymmetric), and the angular resolution of the detector. The width of the folding angle distribution for complete momentum transfer events can be estimated using the kinematics following the Viola systematics [22] for symmetric fission fragments; for the asymmetric fragments the same is done by incorporating the modification of the kinetic energy [26]. Following this idea [27], the widths of the fission fragment folding angle distributions for complete momentum transfer events were calculated. To validate the calculation, the widths of the folding angle distributions were calculated for reactions $p + {}^{238}\text{U}$ and ${}^4\text{He} + {}^{238}\text{U}$, where the ICF component is absent. The folding angle distributions for $p + {}^{238}\text{U}$ and ${}^4\text{He} + {}^{238}\text{U}$ reactions were measured in an experimental campaign at the Variable Energy Cyclotron Centre, Kolkata, and the results will be published elsewhere [28].

In Fig. 2, we show the variation of the ratio of the rms width of the measured and calculated folding angle distributions ($\sigma_{\text{expt}}/\sigma_{\text{cal}}$) with energy ($E_{\text{c.m.}}/V_B$). It can be seen that at the entire measured energy range the ratio is close to 1 for proton- and α -particle-induced reactions as there is no ICF. However, in the ${}^9\text{Be} + {}^{238}\text{U}$ reaction with loosely bound projectiles, it is found that for the inclusive (“ungated”) data, the ratio deviates from unity. It signifies that the measured widths of the fission fragment folding angle distributions are much larger than the calculated values for the complete momentum transfer events. It is also observed that the ratio ($\sigma_{\text{expt}}/\sigma_{\text{cal}}$) increases with decrease in beam energy. This is in sharp contrast to the ${}^{12}\text{C} + {}^{232}\text{Th}$ reaction in which a similar compound nucleus (${}^{244}\text{Cm}$) was populated [29,30], where the experimental folding angle distribution was found to match with the calculated width for complete fusion fission. In the reaction ${}^{12}\text{C} + {}^{232}\text{Th}$

with the tightly bound projectile, there is a minor admixture ($\approx 5\%$) of ICF in the measured energy range [30].

However, the increase in width of the folding angle distributions with decrease in energy as observed in the present measurement in the ${}^9\text{Be} + {}^{238}\text{U}$ reaction at below barrier was also earlier reported in ${}^6\text{Li} + {}^{232}\text{Th}$ [10] and ${}^{6,7}\text{Li} + {}^{238}\text{U}$ [18] reactions. It was indicated that, since ${}^{6,7}\text{Li}$ are loosely bound nuclei, the total fission events had contributions from both CF and ICF processes. The increase in width at lower energies may have contributions from ICF, i.e., breakup fusion and/or transfer-induced fission. Thus, the behavior of the energy dependence of the width of the folding angle distributions for inclusive events in the present measurement is consistent with the data for the loosely bound ${}^{6,7}\text{Li}$ induced reactions [10,11,18].

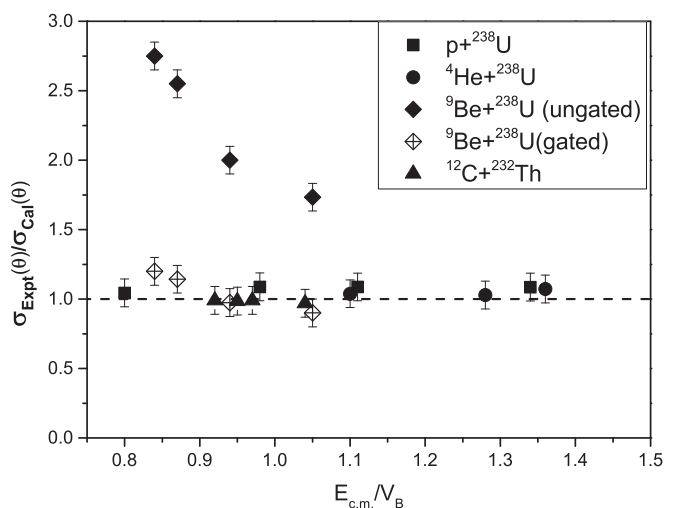


FIG. 2. Variation of the ratio of the rms value of the width of measured and calculated folding angle distributions with energy. $E_{\text{c.m.}}$ is the center of mass energy and V_B is the Coulomb barrier.

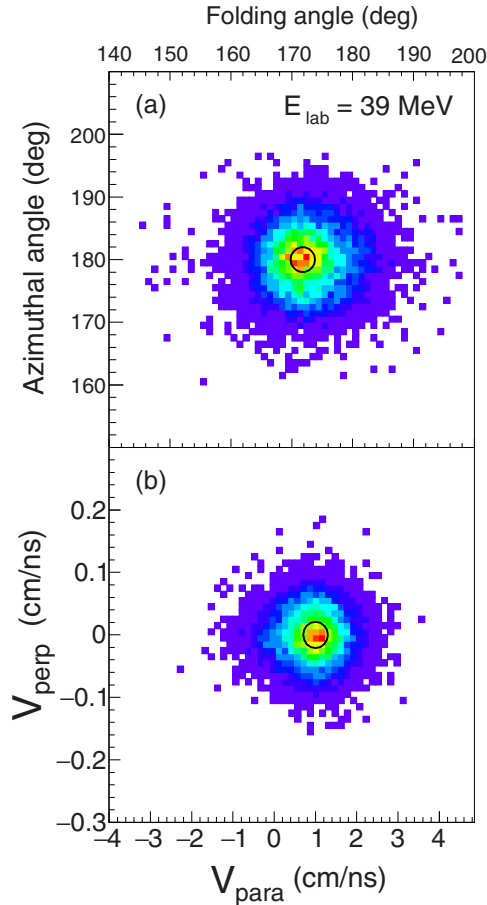


FIG. 3. (a) Measured folding angle distributions of complementary fission fragments and (b) experimentally determined velocity components of the fissioning nuclei for the ${}^9\text{Be} + {}^{238}\text{U}$ reaction at an energy $E_{\text{lab}} = 39\text{ MeV}$. Complete momentum transfer fusion-fission (CF) events lie in the center of the plot, as expected. The black circles indicate the cut used to select the CF events for the determination of mass distribution (see text).

B. Separation of complete and incomplete fusion-fission cross sections

The fission fragments for complete fusion-fission events are usually determined from inclusive experimental data (admixture of CF and ICF) by two methods: (a) from the distributions of polar (θ) and azimuthal (ϕ) angles of the detected fragments, and (b) from the correlation of the velocity of the fissioning system in the beam direction relative to the recoil of the fused system (V_{para}) and the velocity perpendicular to the reaction plane (V_{perp}) [17]. In reactions with tightly bound projectiles, CF and ICF events have been differentiated using these velocity distributions. However, a clear separation was not possible in the present measurement involving loosely bound nuclei as can be seen in Fig. 3. We show in Fig. 3(a) the typical angular correlations of the fragments in θ and ϕ and in Fig. 3(b), the measured distribution of velocity correlation (V_{para} vs V_{perp}) of the fissioning nuclei for the reaction ${}^9\text{Be} + {}^{238}\text{U}$ at $E_{\text{lab}} = 39\text{ MeV}$. Although clear distinction is not possible, the intense peak at the center should correspond

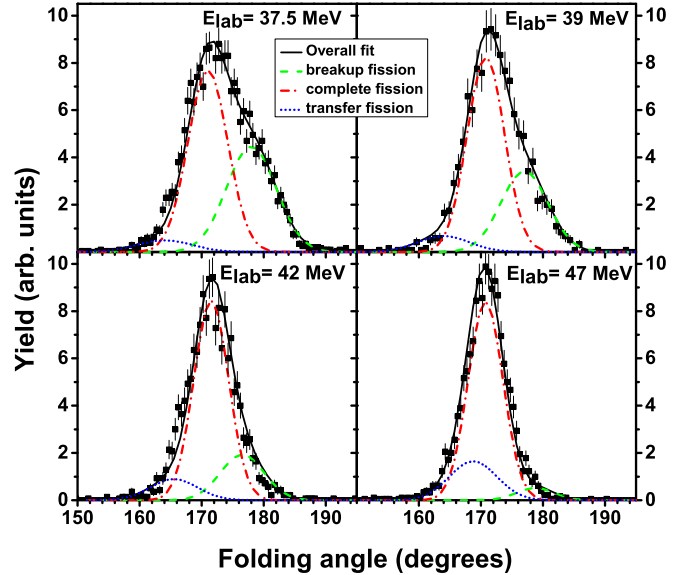


FIG. 4. Folding angle distributions for the reaction ${}^9\text{Be} + {}^{238}\text{U}$ at measured beam energies of $E_{\text{lab}} = 37.5, 39, 42,$ and 47 MeV and decomposition of the folding angle distributions by three Gaussians (see text).

to the CF events. We used a narrow gate, as shown by black contours, to select the possible CF events (a more narrow gate only reduces the statistics). The extracted rms width of the folding angle distributions corresponding to the selected CF events for the ${}^9\text{Be} + {}^{238}\text{U}$ reaction is shown by open symbols (“gated”) in Fig. 2. It can be seen that the values are smaller compared to the inclusive events; however, they show a minor deviation from unity. This indicates that the admixture of ICF is still there even after using the gate and a complete separation of the CF events may not be possible to achieve.

Itkis *et al.* suggested [10] that the contribution of ICF to the total fission cross section can be estimated from the decomposition of the fission fragment folding angle distributions. In ${}^9\text{Be} + {}^{238}\text{U}$ reactions the fission events may be produced in the processes in which a fissioning nucleus is formed in an excitation energy above the fission barrier. Such processes can be (i) complete fusion of ${}^9\text{Be}$ with ${}^{238}\text{U}$, (ii) incomplete fusion, i.e., breakup of ${}^9\text{Be}$ into two ${}^4\text{He}$ atoms and a neutron followed by fusion of one of the fragments, or (iii) direct processes like transfer of a neutron or α particle to the target nucleus.

The measured folding angle distributions for all the events are shown in Fig. 4. The total folding angle distribution comprises both complete fusion fission as well as incomplete fusion fission events. For the complete fusion the entire projectile momentum is transferred to the target and the compound nucleus recoils in the direction of the beam with a momentum equal to that of the incident beam momentum. In the center of mass frame, the fissioning nucleus splits into two fragments moving apart at an angle of 180° . Due to the forward momentum of the recoiling nucleus, the folding angle is less than 180° in the laboratory frame as can be seen in Fig. 4. The peak of the folding angle distribution for symmetric fragments can be estimated kinematically for

complete fusion fission [16,27]. However, for the incomplete fusion, the momentum transferred to the target and the recoil momentum of the composite thus formed differs from the incident beam momentum. This is the primary idea behind using the folding angle as a tool for detection of the presence of ICF in the reaction.

To extract the ICF contribution in total fission cross sections, the folding angle distributions as shown in Fig. 4 were thus fitted with three Gaussians, each corresponding to the fission from three different sources: (i) CF, which is complete fusion of ${}^9\text{Be}$ with ${}^{238}\text{U}$; (ii) transfer-induced fission, which is incomplete fusion of a neutron or α particle with ${}^{238}\text{U}$, whereby the ejectiles go in the backward angles, making the fission fragment folding angle lower than CF; and (iii) breakup capture fission, incomplete fusion of a neutron or α particle with ${}^{238}\text{U}$. Because breakup capture is a two-step process, the ejectiles take away the major part of the beam energy [14], making the folding angle higher than CF. The peak and width of the CF events were estimated using Viola *et al.*'s systematics [22]. The peak and width of the folding angle distribution for the transfer-induced fission would be influenced by the angular distribution of the ejectiles which was presented in Ref. [12], and was constrained while fitting the distributions. At the below-barrier energies, the breakup capture fission is dominated by neutron capture. This is due to the higher cross sections (almost five orders of magnitude) of neutron-induced fission compared to the α -particle-induced fission on ${}^{238}\text{U}$ [31,32]. Neutrons arising from breakup carry only a small part of the incident energy and hence the folding angle peak for breakup fission was found near 180° in the laboratory frame, and the width was treated as a free parameter while fitting. It is observed that for transfer-induced fission, the folding angle peak shifts to higher angles as the beam energy increases.

It is to be mentioned here that fitting of the folding angle distributions at below-barrier energies is not robust as the ejectiles were not detected in this experiment, but simulated from the kinematics. Nevertheless, the available data at the above-barrier energies [12] and additional measurements of fission fragment mass distributions by us at all the energies, as discussed in the later sections, allow us to reliably determine the contribution of incomplete fusion in the total fission cross section.

The contribution of incomplete fusion fission in total fission cross-section was extracted from decompositions of the folding angle distributions and is shown in Fig. 5. For the highest energy at $E_{\text{lab}} = 47\text{ MeV}$ the contribution of ICF is $\approx 25 \pm 4\%$. However, below the Coulomb barrier the contributions of the ICF process increase due to the breakup of ${}^9\text{Be}$ and at the lowest energy, $E_{\text{lab}} = 37.5\text{ MeV}$, the contribution of the ICF process is found to be $\approx 45\%$. From the systematic study of fusion involving nuclides with low binding energy it is reported that the suppression of complete fusion at above-barrier energies is typically by 30% [1,33]. Therefore, it is interesting to note that the observed ICF fraction ($\approx 25 \pm 4\%$) at above-barrier energies is nearly equal to the complete fusion suppression factors for the ${}^9\text{Be} + {}^{238}\text{U}$ reaction. The contribution of ICF in the total fission cross section observed in the present reaction is similar to that

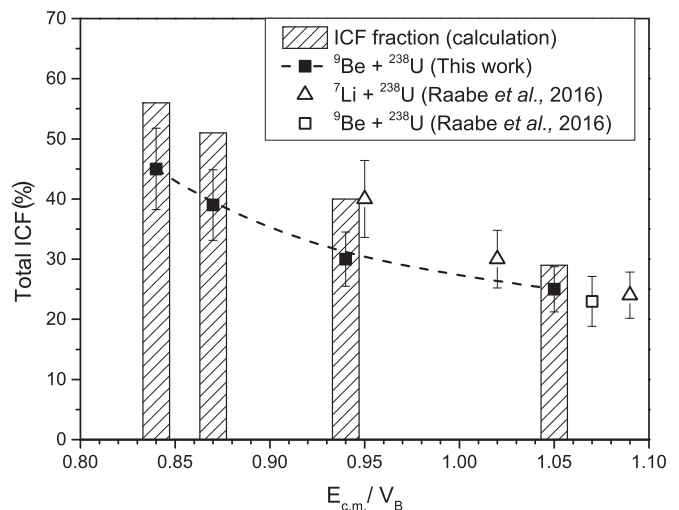


FIG. 5. Calculated incomplete fusion fission (ICF) cross section for the reaction ${}^9\text{Be} + {}^{238}\text{U}$ near the barrier in comparison with the experimental values extracted from the folding angle distributions. The results from the measurements for similar systems [12] are also shown.

of ${}^7\text{Li} + {}^{238}\text{U}$ and ${}^9\text{Be} + {}^{238}\text{U}$ [12] reactions at above-barrier energies.

It is to be mentioned that this experimental study indicates the lower limits of possible admixture of ICF in the total cross section obtained from the decomposition of the fission fragment folding angle distributions. As mentioned earlier, the possible origins of these incomplete fusion channels are breakup of ${}^9\text{Be}$ into a neutron and ${}^8\text{Be}$ (which subsequently decays into two alpha particles) or transfer of a neutron or α particle from the projectile to the target. A theoretical estimation of the possible contribution of the breakup and transfer to the experimental values determined from the folding angle distributions is given in the next section.

The distorted wave Born approximation based theoretical code DWUCK4 [34] was used to estimate the contribution of α -particle transfer reactions, while the coupled reaction channel code FRESKO [35] was used to estimate the breakup contributions and neutron transfer channels. It can be observed from Fig. 5 that the extracted ICF contribution in the total fission cross sections, obtained from the decomposition of fission fragment folding angle distributions, is lower than that predicted by the theoretical calculations (DWUCK4 and FRESKO) as shown by hatch lines. This is because there are some noncapture breakup/transfer events, as well as any non-fission events; thus the result obtained from the folding angle distributions provides the lower limits of the ICF fraction. A complete kinematic measurement of the fission fragments along with any ejectiles may be necessary to understand the detailed reaction mechanisms.

C. Mass distributions

Since separation of CF events could not be completely achieved from the folding angle and velocity distributions (as discussed and shown in Fig. 3), in the first step of the

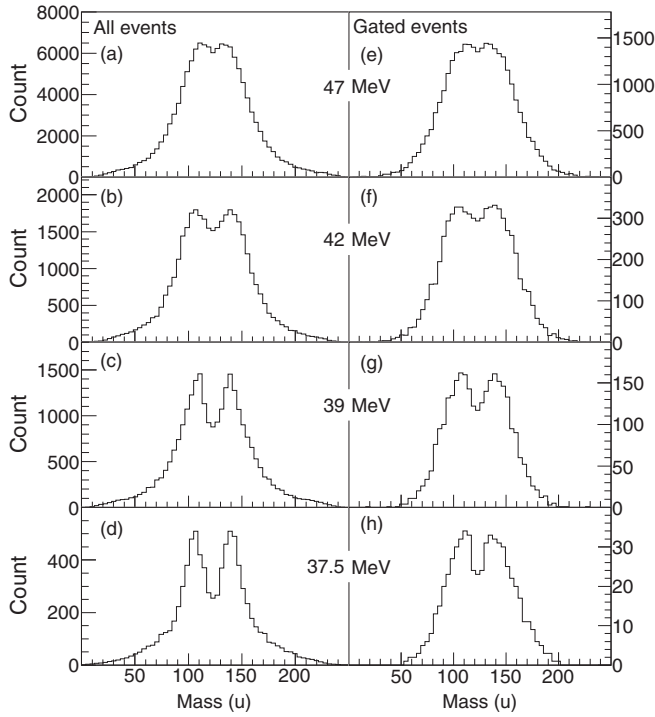


FIG. 6. Fission fragment mass distributions in the reaction ${}^9\text{Be} + {}^{238}\text{U}$. The left panel shows the mass distributions for all events and the right panel is for the gated (as shown by black circles in Fig. 3) events.

calculation of mass distribution, it was assumed that all the events originated from complete fusion of ${}^9\text{Be}$ and ${}^{238}\text{U}$. In the next step, the gated events (possible CF events) as shown in Fig. 3 were analyzed and the mass distributions of the gated events were compared with the mass distributions of all events. The calculated mass distributions assuming all the events originated from CF events are shown in Figs. 6(a)–6(d) at energies $E_{\text{lab}} = 47, 42, 39,$ and 37.5 MeV, respectively. The mass distributions were found to be double humped at the lowest beam energy and gradually become near symmetric with increasing beam energy. In Figs. 6(e)–6(h) the extracted mass distributions for the possible CF events (selected events with gate as shown in Fig. 3) are shown, which also follow similar behavior. However, it is observed that for a particular beam energy, there are more symmetric components in the mass distribution in the gated events compared to those for inclusive events.

The peak-to-valley ratios of the fission fragment mass distributions are extracted at all the energies mentioned above and plotted in Fig. 7 as (black) squares for the inclusive events and (red) triangles for the gated events. With increase in excitation energy, the peak-to-valley ratio decreases both for inclusive and CF events. The value of the peak-to-valley ratio (P/V) is a measure of the degree of nuclear heating. Thus it is clear that with an increase in the beam energy the fissioning nuclei are heated very fast. The measured P/V values are compared with the values calculated using the GEneral description of Fission observables (GEF) code [19,36]. The GEF code is a semiempirical calculation framework that uses parameters

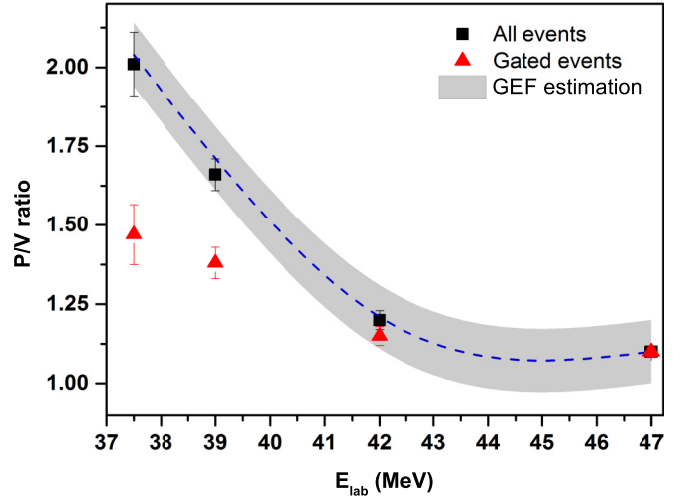


FIG. 7. Variation of the peak-to-valley ratio (P/V) of the measured mass distributions with the beam energy. The blue dashed line denotes the theoretical calculation following GEF [19] considering that the mass distributions have admixture from CF and ICF. The fractions of CF and ICF were extracted from the folding angle analysis as described in this work. The shaded region depicts the uncertainty in the calculation.

which were calculated from the benchmark data. The peak-to-valley ratio was estimated from GEF using the known fraction of the CF and ICF events from the folding angle distribution analysis as described in this work. The energy dependence of the measured P/V value for the inclusive events (“ungated”) could be well reproduced by GEF prediction as shown in Fig. 7.

D. Understanding the mass distributions with two-center shell model calculation

A two-center shell model (TCSM) calculation [20,37,38] was used to explore the impact of ICF events on the fission mass distributions at $E_{\text{lab}} = 47$ MeV. To account for the mass distribution, the driving (adiabatic) potential at the point of contact of the nascent fragments was calculated in the framework of a macro-microscopic TCSM for the reaction ${}^9\text{Be} + {}^{238}\text{U}$ assuming that the reaction only produces the compound nucleus ${}^{247}\text{Cm}$. The temperature dependence of the driving potential was estimated by calculating the ground state shell correction with respect to the liquid drop model [39], and incorporating a temperature dependence in the form of $(\exp(-\gamma U))$ [40], where γ is the shell damping factor and U is the energy available at the saddle point [41]. The Strutinsky hybrid model [32,42] was used to qualitatively estimate the shape of the driving potential at finite temperature. The calculated driving potential at the highest beam energy of 47 MeV is shown as a red line in the lower panel of Fig. 8. As there is no indication of any pocket (or shell effects) at the asymmetric mass in the driving potential, the fission fragment mass distribution is expected to be symmetric and could be described by a single Gaussian [41]. However, the observed mass distribution is clearly asymmetric. This signifies that the asymmetry in the observed mass distribution originates from incomplete fusion. The measured mass distribution could be

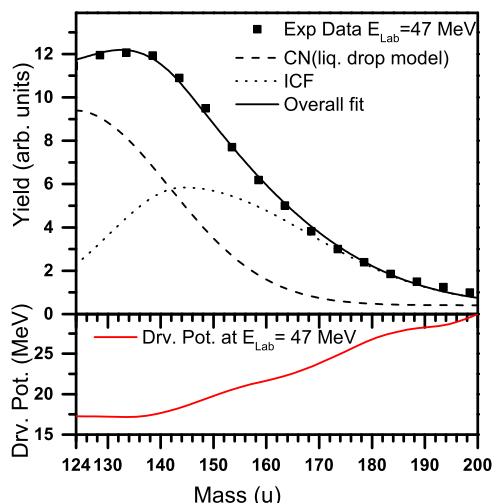


FIG. 8. Top: Half-mass distribution in the fission of ^{247}Cm at 47 MeV. The dashed Gaussian accounts for the symmetric distribution which can be described by the liquid drop model, and the dotted Gaussian could account for incomplete fusion fission events. Together they fit the experimental mass distribution (black line). Bottom: The red line represents the driving potential at the touching configuration calculated using the two-center shell model.

well explained by a symmetric Gaussian following a liquid drop model and an asymmetric Gaussian function arising due to the transfer/breakup-induced ICF. While the fitting parameters for the symmetric Gaussian were entirely determined from the systematics of experimental data [41], only the peak of the asymmetric Gaussian was constrained [30]. The two Gaussians together lead to a best fit of the experimental mass distribution, as shown by the black line in the upper panel of Fig. 8. It is interesting to note that the area of the symmetric Gaussian is $\approx 75\%$ of the total, as also obtained from the folding angle distribution analysis at 47 MeV beam energy. This confirms that the decomposition of the folding angle distributions provides a reliable estimate of ICF fraction.

IV. SUMMARY

The fission fragment folding angle and mass distributions in reaction $^9\text{Be} + ^{238}\text{U}$ are measured near the Coulomb barrier energies. The observed energy dependence of the width of the

folding angle distributions for the present systems was found to be different as compared to the reaction $^{12}\text{C} + ^{232}\text{Th}$ involving tightly bound projectiles producing similar compound nuclei. The results of the present study are consistent with those observed for $^{6,7}\text{Li}$ -induced reactions on actinide targets in which the increase in width of the folding angle distributions was due to the contributions from projectile-breakup-and/or transfer-induced fission.

The variation of the peak-to-valley ratio of the mass distributions of inclusive events was found to sharply increase with decreasing beam energy. As the peak-to-valley ratio is a measure of nuclear heating of the composite system, the sharp increase of the measured peak-to-valley ratio with decreasing beam energy indicates the population of composite nuclei with relatively lower excitation energy than expected. This signifies the possible contribution of incomplete fusion fission (transfer- or breakup-induced fission) where part of the projectile fuses and the composite nuclei are formed with less excitation energy. Selecting the events in the distributions of the velocity components of the composite nuclei, the probable complete fusion-fission events were derived. The contributions of the incomplete fusion were extracted from the analysis of the folding angle distributions. At the above-barrier energies, the incomplete fusion was found to be $\approx 25\%$ of the total fusion cross section, which is similar to the complete fusion suppression factor for reactions with loosely bound projectiles. The variation of the peak-to-valley ratio of the mass distributions with energy could be explained by semiempirical calculation using GEF, considering the admixture of CF and ICF events. Coincidence measurements of the fission fragments with the reaction products will provide a better understanding of the reaction dynamics.

ACKNOWLEDGMENTS

Illuminating discussions with P. Bhattacharya, Subinit Roy, and S. Santra are gratefully acknowledged. One of the authors (D.P.) would like to thank Sumit Saha and Sanchari Thakur for helpful discussions on the ROOT software. S.B. acknowledges with thanks the financial support received as the Raja Ramanna Fellow from the Department of Atomic Energy, Government of India. The authors are thankful to the staffs of BARC-TIFR Pelletron Facility in Mumbai, India, for providing high quality beams for the experiment and acknowledge the support of the Department of Atomic Energy, Government of India, under Project No. 12P-R&D-TFR-5.02-0300.

- [1] K. J. Cook, E. C. Simpson, L. T. Bezzina, M. Dasgupta, D. J. Hinde, K. Banerjee, A. C. Berriman, and C. Sengupta, *Phys. Rev. Lett.* **122**, 102501 (2019).
- [2] V. Jha, V. V. Parkar, and S. Kailas, *Phys. Rep.* **845**, 1 (2020), and references therein.
- [3] G. S. Li, J. G. Wang, J. Lubian, H. O. Soler, Y. D. Fang, M. L. Liu, N. T. Zhang, X. H. Zhou, Y. H. Zhang, B. S. Gao, Y. H. Qiang, S. Guo, S. C. Wang, K. L. Wang, K. K. Zheng, R. Li, and Y. Zheng, *Phys. Rev. C* **100**, 054601 (2019).
- [4] K. J. Cook, I. P. Carter, E. C. Simpson, M. Dasgupta, D. J. Hinde, L. T. Bezzina, S. Kalkal, C. Sengupta, C. Simenel, B. M. A. Swinton-Bland, K. Vo-Phuoc, and E. Williams, *Phys. Rev. C* **97**, 021601(R) (2018).
- [5] D. Luong, M. Dasgupta, D. Hinde, R. du Rietz, R. Rafiei, C. Lin, M. Evers, and A. Diaz-Torres, *Phys. Lett. B* **695**, 105 (2011).
- [6] K. Hagino, A. Vitturi, C. H. Dasso, and S. M. Lenzi, *Phys. Rev. C* **61**, 037602 (2000).

- [7] M. S. Hussein, M. P. Pato, and A. F. R. de Toledo Piza, *Phys. Rev. C* **51**, 846 (1995).
- [8] R. Raabe, J. L. Sida, J. L. Charvet, N. Alamanos, C. Angulo, J. M. Casadjan, S. Courtin, A. Drouart, D. J. C. Durand, P. Figuera *et al.*, *Nature (London)* **823**, 431 (2004).
- [9] L. F. Canto, P. R. S. Gomes, R. Donangelo, and M. S. Hussein, *Phys. Rep.* **424**, 1 (2006).
- [10] I. M. Itkis, A. A. Bogachev, A. Y. Chizhov, D. M. Gorodisskiy, M. G. Itkis, G. N. Knyazheva, N. A. Kondratiev, E. M. Kozulin, L. Krupa, S. I. Mulgin *et al.*, *Phys. Lett. B* **640**, 23 (2006).
- [11] A. Pal, S. Santra, D. Chattopadhyay, A. Kundu, A. Jhingan, P. Sugathan, B. K. Nayak, A. Saxena, and S. Kailas, *Phys. Rev. C* **99**, 024620 (2019).
- [12] R. Raabe, C. Angulo, J. L. Charvet, C. Jouanne, L. Nalpas, P. Figuera, D. Pierroutsakou, M. Romoli, and J. L. Sida, *Phys. Rev. C* **74**, 044606 (2006).
- [13] S. Dubey, S. Mukherjee, D. C. Biswas, B. K. Nayak, D. Patel, G. K. Prajapati, Y. K. Gupta, B. N. Joshi, L. S. Danu, S. Mukhopadhyay, B. V. John, V. V. Desai, S. V. Suryanarayana, R. P. Vind, N. N. Deshmukh, S. Appannababu, and P. M. Prajapati, *Phys. Rev. C* **89**, 014610 (2014).
- [14] V. Tripathi, A. Navin, V. Nanal, R. G. Pillay, K. Mahata, K. Ramachandran, A. Shrivastava, A. Chatterjee, and S. Kailas, *Phys. Rev. C* **72**, 017601 (2005).
- [15] A. Shrivastava, A. Navin, A. Diaz-Torres, V. Nanal, K. Ramachandran, M. Rejmund, S. Bhattacharyya, A. Chatterjee, S. Kailas, A. Lemasson, R. Palit, V. Parkar, R. Pillay, P. Rout, and Y. Sawant, *Phys. Lett. B* **718**, 931 (2013).
- [16] N. Majumdar, P. Bhattacharya, D. C. Biswas, R. K. Choudhury, D. M. Nadkarni, and A. Saxena, *Phys. Rev. C* **51**, 3109 (1995).
- [17] D. J. Hinde, M. Dasgupta, J. R. Leigh, J. C. Mein, C. R. Morton, J. O. Newton, and H. Timmers, *Phys. Rev. C* **53**, 1290 (1996).
- [18] S. Santra, A. Pal, P. K. Rath, B. K. Nayak, N. L. Singh, D. Chattopadhyay, B. R. Behera, V. Singh, A. Jhingan, P. Sugathan, K. S. Golda, S. Sodaye, S. Appannababu, E. Prasad, and S. Kailas, *Phys. Rev. C* **90**, 064620 (2014).
- [19] B. Jurado and K. H. Schmidt, Computer code GEF, Version 1.2, 2016, <http://www.khs-erzhausen.de/GEF-2016-1-2.html>.
- [20] V. I. Zagrebaev *et al.*, *Phys. Part. Nucl.* **38**, 469 (2007).
- [21] D. C. Biswas *et al.*, *Nucl. Instrum. Methods Phys. Res. A* **901**, 76 (2018).
- [22] V. E. Viola, K. Kwiatkowski, and M. Walker, *Phys. Rev. C* **31**, 1550 (1985).
- [23] T. K. Ghosh *et al.*, *Nucl. Instrum. Methods Phys. Res. A* **540**, 285 (2005).
- [24] D. Paul, A. Sen, T. K. Ghosh, Md. Moin Shaikh, K. Atreya, S. Kundu, K. Banerjee, C. Bhattacharya, S. Bhattacharya, J. K. Meena, D. C. Biswas, B. N. Joshi, N. Kumar, G. K. Prajapati, Y. K. Gupta, K. Mahata, K. Ramachandran, and S. Pal, *Phys. Rev. C* **102**, 054604 (2020).
- [25] A. Pal, S. Santra, D. Chattopadhyay, A. Kundu, A. Jhingan, P. Sugathan, N. Saneesh, M. Kumar, N. L. Singh, A. Yadav *et al.*, *Phys. Rev. C* **98**, 031601(R) (2018).
- [26] S. I. Mulgin, V. N. Okolovich, and S. V. Zhdanova, *Phys. Lett. B* **462**, 29 (1999).
- [27] P. Bhattacharya *et al.*, *Nuovo Cimento A* **108**, 819 (1995).
- [28] K. Atreya, A. Sen, T. K. Ghosh, Md. Moin Shaikh, Samir Kundu, T. K. Rana, K. Banerjee, and C. Bhattacharya (unpublished).
- [29] T. K. Ghosh *et al.*, *Phys. Lett. B* **627**, 26 (2005).
- [30] T. K. Ghosh, Ph.D. thesis, Jadavpur University, 2005 (unpublished); [arXiv:nucl-ex/0508009](https://arxiv.org/abs/nucl-ex/0508009) [nucl-ex].
- [31] M. Trotta, J. L. Sida, N. Alamanos, A. Andreyev, F. Auger, D. L. Balabanski, C. Borcea, N. Coulier, A. Drouart, D. J. C. Durand, G. Georgiev, A. Gillibert, J. D. Hinnefeld, M. Huysse, C. Jouanne, V. Lapoux, A. Lépine, A. Lumbroso, F. Marie, A. Musumarra, G. Neyens, S. Ottini, R. Raabe, S. Ternier, P. Van Duppen, K. Vyvey, C. Volant, and R. Wolski, *Phys. Rev. Lett.* **84**, 2342 (2000).
- [32] R. Vandenbosch and J. R. Huizenga, *Nuclear Fission* (Academic, New York, 1973).
- [33] M. Dasgupta, D. J. Hinde, R. D. Butt, R. M. Anjos, A. C. Berriman, N. Carlin, P. R. S. Gomes, C. R. Morton, J. O. Newton, A. Szanto de Toledo, and K. Hagino, *Phys. Rev. Lett.* **82**, 1395 (1999).
- [34] P. D. Kunz, DWUCK4 computer code, *Organisation for Economic Co-Operation and Development, Nuclear Energy Agency, Issy-les-Moulineaux*, France, 1996.
- [35] I. J. Thompson, *Comput. Phys. Rep.* **7**, 167 (1988).
- [36] K.-H. Schmidt, B. Jurado, C. Amouroux, and C. Schmitt, *Nucl. Data Sheets* **131**, 107 (2016).
- [37] U. Mosel and H. Schmitt, *Phys. Rev. C* **4**, 2185 (1971).
- [38] J. Maruhn and W. Greiner, *Z. Phys. A* **251**, 431 (1972).
- [39] V. I. Zagrebaev, A. S. Denikin, A. V. Karpov, A. P. Alekseev, M. A. Naumenko, V. A. Rachkov, V. V. Samarin, and V. V. Saiko, NRV web knowledge base on low-energy nuclear physics, <http://nrv.jinr.ru/>.
- [40] A. V. Ignatyuk, G. N. Smirenkin, and A. S. Tishin, *Yad. Fiz.* **21**, 485 (1975).
- [41] M. G. Itkis, N. A. Kondratiev, S. I. Mulgin, V. N. Okolovich, A. Y. Rusanov, and G. N. Smirenkin, *Yad. Fiz.* **53**, 1225 (1991).
- [42] V. M. Strutinsky, *Nucl. Phys. A* **95**, 420 (1967).